# EquiPocket: an E(3)-Equivariant Geometric Graph Neural Network for Ligand Binding Site Prediction

**Yang Zhang** [1] **Zhewei Wei** [1] **Ye Yuan** [2] **Chongxuan Li** [1] **Wenbing Huang** [1]

## Abstract

Predicting the binding sites of target proteins plays a fundamental role in drug discovery. Most existing deep-learning methods consider a protein as a 3D image by spatially clustering its atoms into voxels and then feed the voxelized protein into a 3D CNN for prediction. However, the CNN-based methods encounter several critical issues: 1) defective in representing irregular protein structures; 2) sensitive to rotations; 3) insufficient to characterize the protein surface; 4) unaware of protein size shift. To address the above issues, this work proposes EquiPocket, an E(3)-equivariant Graph Neural Network (GNN) for binding site prediction, which comprises three modules: the first one to extract local geometric information for each surface atom, the second one to model both the chemical and spatial structure of protein and the last one to capture the geometry of the surface via equivariant message passing over the surface atoms. We further propose a dense attention output layer to alleviate the effect incurred by variable protein size. Extensive experiments on several representative benchmarks demonstrate the superiority of our framework to the state-of-the-art methods. Related codes can be found at the link `https://github.com/fengyuewuya/EquiPocket`.

## 1. Introduction

Nearly all biological and pharmacological processes in living systems involve interactions between receptors (*i.e.* target proteins) and ligands (*i.e.* small molecules) (Rang, 2006). These interactions take place at specific regions that are referred to as binding sites/pockets on the target protein structures. In-silico ligand binding site prediction forms an indispensable and even the first step for various tasks. For example, the predicted binding sites (or pockets) on the protein greatly facilitates downstream tasks, including protein-ligand docking (Zhang et al., 2022; Yang et al., 2023) and structure-based molecular generation (Isert et al., 2023).

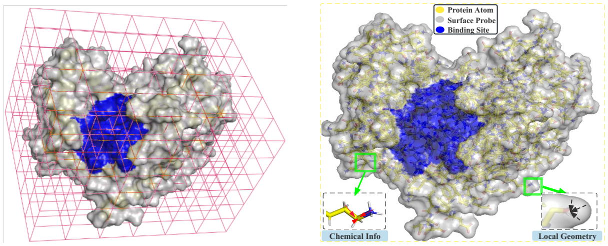

(a) CNN-based methods (b) Our EquiPocket

Figure 1: Illustrative comparison between previous CNN-based methods (voxelization) and our EquiPocket.

Through the past years, various computational methods for ligand binding site detection have emerged, broadly categorized (Macari et al., 2019) into geometry-based (Levitt & Banaszak, 1992; Le Guilloux et al., 2009; Dias et al., 2017), probe-based (Laurie & Jackson, 2005; Faller et al., 2015), and template-based methods (Brylinski & Skolnick, 2008; Toti et al., 2018). These methods exploit hand-crafted algorithms guided by domain knowledge or external templates, leading to insufficient expressivity in representing proteins. Lately, machine-learning methods like P2rank (Krivák & Hoksza, 2018) utilize Random Forest with surface geometry for prediction, which are still limited by the hand-crafted features and insufficiently-expressive models. Motivated by the breakthrough of deep learning, Convolutional Neural Networks (CNNs) have been applied successfully for ligand binding site prediction (Kandel et al., 2021). Typical works include DeepSite (Jiménez et al., 2017), DeepPocket (Aggarwal et al., 2021), DeepSurf (Mylonas et al., 2021), RecurPocket (Li et al., 2022) and etc (Semwal et al., 2023). The CNN-based methods consider a protein as a 3D image by spatially clustering its atoms into the nearest voxels, and then model the binding site prediction as a object detection

[1] Gaoling School of Artificial Intelligence, Renmin University of China, beijing, China [2] Beijing Institute of Technology, China. Correspondence to: Zhewei Wei <zhewei@ruc.edu.cn>, Wenbing Huang <hwenbing@ruc.edu.cn>.

*Proceedings of the 41st International Conference on Machine Learning*, Vienna, Austria. PMLR 235, 2024. Copyright 2024 by the author(s).

problem or a semantic segmentation task on 3D grids. These methods have demonstrated superiority and tend to achieve top performance on various public benchmarks (Mylonas et al., 2021). In spite of the impressive progress, existing CNN-based methods still encounter several issues:

**Issue 1.** Defective in leveraging regular voxels to model the proteins of irregular shape (see Figure 1(a)). Moreover, the voxelization is usually constrained within a fixed-size (*e.g.* 70Å × 70Å × 70Å ) (Stepniewska-Dziubinska et al., 2020). The outside atoms will be directly discarded, resulting in incomplete and inaccurate modeling for large proteins.

**Issue 2.** Sensitive to rotations. The CNN-based methods rely on fixed coordinate bases for discretizing proteins into 3D grids. When rotating the protein, the voxelization results could be distinct, affecting predicted binding sites. This contradicts the fact that any protein rotation keeps the binding sites invariant. While it can be alleviated by local grid (Mylonas et al., 2021) or augmenting data with random rotations (Ragoza et al., 2017), which yet is data-dependent and unable to guarantee rotation invariance in theory.

**Issue 3.** Insufficient to characterize the geometry of the protein surface. Surface atoms comprise the major part of the binding pocket, which should be elaborately modeled. In the CNN-based methods, surface atoms are situated within voxels surrounded by empty voxels, which somehow encodes the surface geometry. Nevertheless, such information is too coarse to depict how surface atoms interact and what their local geometry is. Indeed, the description of surface atoms is purely driven by the geometric shape of the solvent-accessible surface of the protein (Richmond, 1984) (Figure 1(b)), which, unfortunately, is less explored in current learning-based works.

**Issue 4.** Unaware of protein size shift. In practical scenarios, the size of proteins varies greatly across different datasets. It requires the deep learning model we apply to be well generalizable and adaptive, so that it is able to overcome the distribution shift incurred by the variable protein size. However, this point is not seriously discussed previously.

To address the above issues, this paper proposes to apply Graph Neural Networks (GNNs) (Kip & Welling, 2016; Chen et al., 2020) instead of CNNs to represent proteins. By considering atoms as nodes, interactions as edges, GNNs are able to encode the irregular protein structures. More importantly, a recent line of researches (Satorras et al., 2021a; Kong et al., 2023) has enhanced GNNs by encapsulating E(3)-equivariance/invariance with respect to translations/rotations; in this way, equivariant GNNs yield outputs that are independent of the choice of the coordinate systems. That being said, trivially applying equivariant GNNs for the binding site prediction task is still incapable of providing desirable performance, and even achieves worse accuracy than the CNN-based counterparts. By looking into their design, equivariant GNNs naturally cope with the first two issues as mentioned above, yet leave the other two unsolved. To this end, we make the contributions as follows:

1) To the best of our knowledge, we are the first to apply an E(3)-equivariant GNN for ligand binding site prediction, which is dubbed **EquiPocket**. In contrast to conventional CNN-based methods, EquiPocket is free of the voxelization process, able to model irregular protein structures by nature, and insensitive to any Euclidean transformation, thereby addressing Issue 1 and 2.

2) EquiPocket consists of three modules: the first one to extract local geometric information for each surface atom with the help of the solvent-accessible surface technique (Richmond, 1984), the second one to model both the chemical and the spatial structures of the protein, and the last one to capture the comprehensive geometry of the surface via equivariant message passing over the surface atoms. The first and the last modules are proposed to tackle Issue 3.

3) To alleviate the effect by protein size shift in Issue 4, we further propose a novel output layer called *dense attention output layer*, which enables us to adaptively balance the scope of the receptive field for each atom based on the density distribution of the neighbor atoms.

4) Extensive experiments demonstrate the superiority of our framework to the SOTA methods in prediction accuracy. The design of our model is sufficiently ablated as well.

It is worth mentioning that some researchers have adopted typical GNNs for protein pocket-related tasks. PocketMiner (Meller et al., 2023) utilizes a graph model to predict where cryptic pockets are likely to open in molecular dynamics simulations. NodeCoder (Abdollahi et al., 2023) predicts protein residue types with a graph representation. ScanNet (Tubiana et al., 2022) is trained to detect protein-protein and protein-antibody binding sites. SiteRadar (Evteev et al., 2023) incorporates grid generation and cropping with GNNs. However, most of these methods significantly differ from the task of ligand binding site prediction in this paper, and moreover, these models are non-equivariant and not geometry-aware. Detailed related work in Appendix A.2.

## 2. Notations and Definitions

**Protein Graph.** A protein such as the example in Figure 1(b) is denoted as a graph $\mathcal{G}_P = (\mathcal{V}_P, \mathcal{E}_C, \mathcal{E}_D)$, where $\mathcal{V}_P = \{v_0, ..., v_N\}$ forms the set of $N$ atoms, $\mathcal{E}_C$ represents the chemical-bond edges, and $\mathcal{E}_D$ collects the spatial edges between any two atoms if their spatial distance is less than a cutoff $\theta > 0$. In particular, each node (*i.e.* atom) is associated with a feature $(\boldsymbol{x}_i, \boldsymbol{c}_i)$, where $\boldsymbol{x}_i \in \mathbb{R}^3$ denotes the 3D coordinates and $\boldsymbol{c}_i \in \mathbb{R}^5$ is the chemical feature.

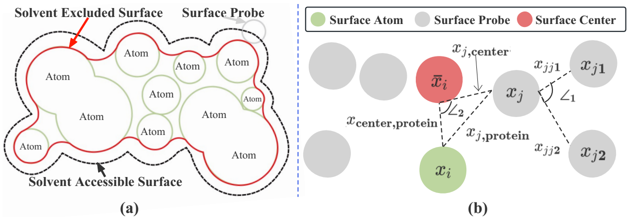

Figure 2: Surface probe (a) and local geometric features (b).

**Surface Probe Set.** The surface geometry of a protein is of crucial interest for binding site detection. By employing the open source MSMS (Sanner et al., 1996), as shown in Figure 2 (a), we move a probe (the grey circle) of a certain radius along the protein to calculate the Solvent Accessibility Surface (SAS) and Solvent Excluded Surface (SES) (Lee & Richards, 1971). The resulting coordinates of probe are considered as surface probes. Here we define the set of surface probes, by $\mathbb{S} = \{s_0, ..., s_M\}$, $M \gg N$. Each surface probe $s_i$ corresponds to $(\boldsymbol{x}_i, p_i)$, where $\boldsymbol{x}_i \in \mathbb{R}^3$ represents the 3D coordinates of $s_i$ and $p_i \in \mathcal{V}_P$ indicates the index of the nearest protein atom in $\mathcal{V}_P$ to $s_i$.

**Protein Surface Graph.** Referring to the surface probes defined above, we collect all the nearest protein atoms $p_i$ of the surface probes, forming the surface graph $\mathcal{G}_S = (\mathcal{V}_S, \mathcal{E}_S)$, and clearly $\mathcal{G}_S \subseteq \mathcal{G}_P$. Notably, the edges of the surface graph, *i.e.* , $\mathcal{E}_S$ is only composed of spatial edges from $\mathcal{E}_D$, since those chemical edges are mostly broken among the extracted atoms.

**Equivariance and Invariance.** In 3D space, the symmetry of the physical laws requires the detection model to be equivariant with respect to arbitrary coordinate systems (Han et al., 2022). In form, suppose $\boldsymbol{X}$ to be 3D geometric vectors (positions, velocities, etc) that are steerable by E(3) group (rotations/translations/reflections), and $\boldsymbol{h}$ non-steerable features. The function $f$ is E(3)-equivariant, if for any transformation $g \in \text{E}(3)$, $f(g \cdot \boldsymbol{X}, \boldsymbol{h}) = g \cdot f(\boldsymbol{X}, \boldsymbol{h})$, $\forall \boldsymbol{X} \in \mathbb{R}^{3\times m}, \boldsymbol{h} \in \mathbb{R}^d$. Similarly, $f$ is invariant if $f(g \cdot \boldsymbol{X}, \boldsymbol{h}) = f(\boldsymbol{X}, \boldsymbol{h})$. The group action $\cdot$ is instantiated as $g \cdot \boldsymbol{X} := \boldsymbol{X} + \boldsymbol{b}$ for translation $\boldsymbol{b} \in \mathbb{R}^3$ and $g \cdot \boldsymbol{X} := \boldsymbol{O}\boldsymbol{X}$ for rotation/reflection $\boldsymbol{O} \in \mathbb{R}^{3\times 3}$.

**Problem Statement.** Given a protein $\mathcal{G}_P$, its surface probes $\mathbb{S}$, and constructed surface graph $\mathcal{G}_S$, our goal is to learn an E(3)-invariant model $f(\mathcal{G}_P, \mathbb{S}, \mathcal{G}_S)$ to predict the atoms of binding sites: $\mathcal{V}_B \subseteq \mathcal{V}_P$.

## 3. The Proposed Methodology

Figure 3 illustrates the overall framework of our EquiPocket, which consists of three modules: the *local geometric modeling module* § 3.1 that focuses on extracting the geometric information of each surface atom, the *global structure modeling module* § 3.2 to characterize both the chemical and spatial structures of the protein, and the *surface message passing module* § 3.3 which concentrates on capturing the entire surface geometry based on the extracted information by the two former modules. The training losses are also presented. The related codes are provided at the link `https://github.com/fengyuewuya/EquiPocket`.

### 3.1. Local Geometric Modeling Module

This subsection presents how to extract the local geometric information of the protein surface $\mathcal{G}_S$, with the help of surface probes $\mathbb{S}$. The local geometry of each protein atom closely determines if the region nearby is appropriate or not to become part of binding sites. In Figure 2 (b), we adopt the surrounding surface probes of each protein surface atom to describe the local geometry. To be specific, for every surface atom $i \in \mathcal{V}_S$, its surrounding surface probes are returned by a subset of $\mathbb{S}$, namely, $\mathbb{S}_i = \{s_j = (\boldsymbol{x}_j, p_j) \in \mathbb{S} \mid p_j = i\}$, where $p_j$, indicates the nearest protein atom. We now construct the geometric information based on $\mathbb{S}_i$. We denote the center/mean of all 3D coordinates in $\mathbb{S}_i$ as $\bar{\boldsymbol{x}}_i$. For each surrounding surface probe $s_j \in \mathbb{S}_i$, we first search its two nearest surface probes from $\mathbb{S}$ as $s_{j_1}$ and $s_{j_2}$, and then calculate the following relative position vectors:

$$\begin{aligned}&\boldsymbol{x}_{jj_1} = \boldsymbol{x}_j - \boldsymbol{x}_{j_1}, \boldsymbol{x}_{jj_2} = \boldsymbol{x}_j - \boldsymbol{x}_{j_2}, \boldsymbol{x}_{j,\text{center}} = \boldsymbol{x}_j - \bar{\boldsymbol{x}}_i,\\ &\boldsymbol{x}_{j,\text{protein}} = \boldsymbol{x}_j - \boldsymbol{x}_i, \boldsymbol{x}_{\text{center,protein}} = \bar{\boldsymbol{x}}_i - \boldsymbol{x}_i.\end{aligned} \tag{1}$$

We further derive the following scalars upon Eq. 1:

$$\begin{aligned}\boldsymbol{g}(s_j) := [&\|\boldsymbol{x}_{jj_1}\|_2, \|\boldsymbol{x}_{jj_2}\|_2, \angle_1,\\ &\|\boldsymbol{x}_{j,\text{center}}\|_2, \|\boldsymbol{x}_{j,\text{protein}}\|_2, \|\boldsymbol{x}_{\text{protein,center}}\|_2, \angle_2],\end{aligned} \tag{2}$$

where the angels are computed by $\angle_1 = \frac{\boldsymbol{x}_{jj_1} \cdot \boldsymbol{x}_{jj_2}}{\|\boldsymbol{x}_{jj_1}\|_2 \|\boldsymbol{x}_{jj_2}\|_2}$ and $\angle_2 = \frac{\boldsymbol{x}_{j,\text{center}} \cdot \boldsymbol{x}_{\text{center,protein}}}{\|\boldsymbol{x}_{j,\text{center}}\|_2 \|\boldsymbol{x}_{\text{center,protein}}\|_2}$; here the operator $\cdot$ defines the inner-product between two vectors. Basically, as displayed in Figure 2, the first three quantities in $\boldsymbol{g}(s_j)$ depict how the nearby surface probes are arranged around $s_j$, and the last four ones describe where $s_j$ is located within the global region of $\mathbb{S}_i$. We aggregate the geometric information $\boldsymbol{g}(s_j)$ over all surface probes in $\mathbb{S}_i$ and obtain a readout descriptor for surface atom $i$ as

$$\begin{aligned}\boldsymbol{g}_i =&[\text{Pooling}(\{\text{MLP}(\boldsymbol{g}(s_j))\}_{s_j \in \mathbb{S}_i}),\\ &\text{MLP}(\text{Pooling}\{(\boldsymbol{g}(s_j))\}_{s_j \in \mathbb{S}_i})].\end{aligned} \tag{3}$$

Here, MLP denotes multi-layer perceptron, and the function Pooling is implemented by concatenating mean and max pooling in our experiments. The front part in Eq. 3 is used to gather local geometric features, while the latter part attempts to compute the global size of surrounding surface probes. Notably, the geometric descriptor $\boldsymbol{g}_i$ is E(3)-invariant.

### 3.2. Global Structure Modeling Module

This module aims at processing the information of the whole protein $\mathcal{G}_P$, including atom type, chemical bonds, relevant

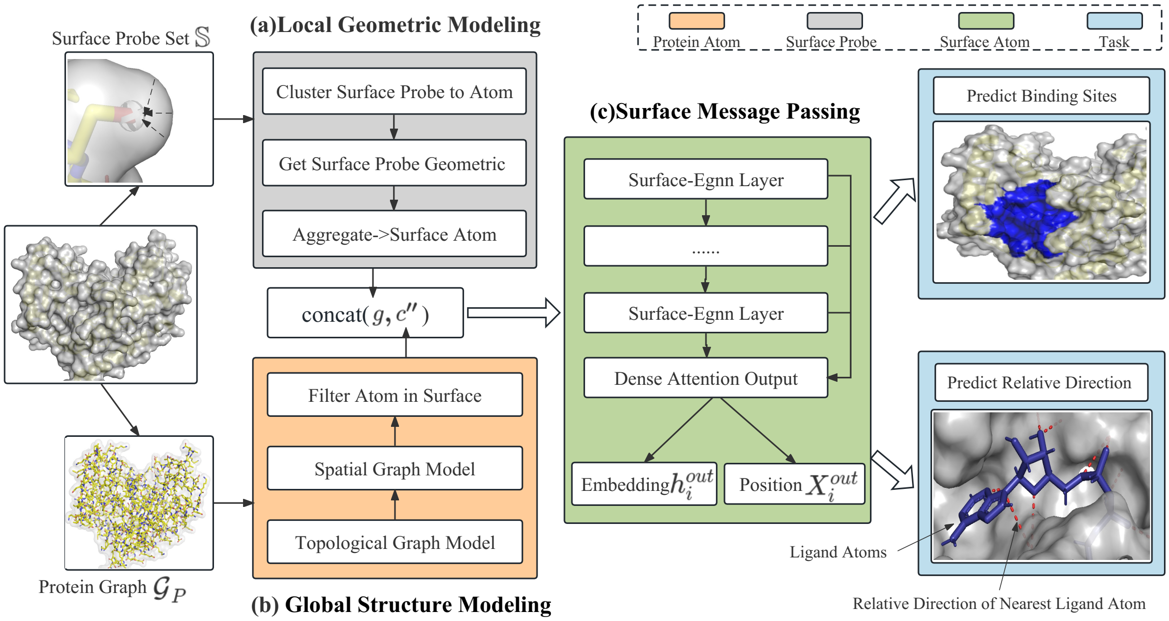

Figure 3: An illustration of the scheme of our EquiPocket framework.

spatial positions, etc. Although the pocket is majorly comprised of surface atoms, the global structure of the protein in general influences how the ligand is interacted with and how the pocket is formulated, which should be modeled. We fulfil this purpose via two concatenated processes: chemical-graph modeling and spatial-graph modeling.

The chemical-graph modeling process copes with the chemical features $\{\boldsymbol{c}_i\}_{i\in\mathcal{V}_P}$ and the chemical interactions $\mathcal{E}_C$ of the protein graph. For each atom in the protein, its chemical type, the numbers of electrons around, and the chemical bonds connected to other atoms are important clues to identify the interaction between the protein and the ligand (Zhang et al., 2022). We employ typical GNNs (Kipf & Welling, 2016; Velikovi et al., 2017; Sabrina et al., 2018) to distill this type of information. Formally, we proceed:

$$\{\boldsymbol{c}'_i\}_{i\in\mathcal{V}_P} = \text{GNN}(\{\boldsymbol{c}_i\}_{i\in\mathcal{V}_P}, \mathcal{E}_C), \tag{4}$$

where $\boldsymbol{c}'_i$ is the updated chemical feature for atom $v_i$. While various GNNs can be used in Eq. 4, here we implement GAT (Velikovi et al., 2017) given its desirable performance observed in our experiments.

The spatial-graph modeling process further involves the 3D coordinates $\{\boldsymbol{x}_i\}_{i\in\mathcal{V}_P}$ to better depict the spatial interactions $\mathcal{E}_D$ within the protein. Different from chemical features $\boldsymbol{c}'_i$, the 3D coordinates provide the spatial position of each atom and reflect the pair-wise distances in 3D space, which is helpful for physical interaction modeling. We leverage EGNN (Satorras et al., 2021a) as it conforms to E(3)-equivariance/invariance and achieves promising performance on modeling spatial graphs:

$$\{\boldsymbol{c}''_i\}_{i\in\mathcal{V}_P} = \text{EGNN}(\{\boldsymbol{x}_i, \boldsymbol{c}'_i\}_{i\in\mathcal{V}_P}, \mathcal{E}_D). \tag{5}$$

Here, we only reserve the invariant output (*i.e.* , $\boldsymbol{c}''_i$) and have discarded the equivariant output (*e.g.* updated 3D coordinates) of EGNN, since the goal of this module is to provide invariant features. We select the updated features of the surface atoms $\mathcal{V}_S$ and fed into the module in § 3.3.

### 3.3. Surface Message Passing Module.

Given the local geometric features $\{\boldsymbol{g}_i\}_{i\in\mathcal{V}_S}$ from § 3.1, and the globally-encoded features of the surface atoms $\{\boldsymbol{c}''_i\}_{i\in\mathcal{V}_S}$ from § 3.2, the module in this subsection carries out equivariant message passing on the surface graph $\mathcal{G}_S$ to renew the entire features of the protein surface. We mainly focus on the surface atoms here, because firstly the surface atoms are more relevant to the binding sites than the interior atoms, and secondly the features $\{\boldsymbol{c}''_i\}_{i\in\mathcal{V}_S}$ that are considered as the input have somehow encoded the information of the interior structure via the processes in § 3.2.

**Surface-EGNN.** During the $l$-th layer message passing, each node is associated with an invariant feature $\boldsymbol{h}_i^{(l)} \in \mathbb{R}^{m_l}$ and an equivariant double-channel matrix $\boldsymbol{X}_i^{(l)} \in \mathbb{R}^{3\times 2}$. We first concatenate $\boldsymbol{c}''_i$ with $\boldsymbol{g}_i$ as the initial invariant feature, $\boldsymbol{h}_i^{(0)} = [\boldsymbol{c}''_i, \boldsymbol{g}_i]$. The equivariant matrix $\boldsymbol{X}_i^{(0)}$ is initialized by the 3D coordinates of the atom and the center of its surrounding surface probes, that is, $\boldsymbol{X}_i^{(0)} = [\boldsymbol{x}_i, \bar{\boldsymbol{x}}_i]$. We update $\boldsymbol{h}_i^{(l)} \in \mathbb{R}^{d_l}$ and $\boldsymbol{X}_i^{(l)} \in \mathbb{R}^{3\times 2}$ synchronously to unveil both the topological and geometrical patterns. Inspired from EGNN (Satorras et al., 2021a) and its multi-channel version GMN (Huang et al., 2022), we formulate the $l$-th layer for each surface atom $i \in \mathcal{V}_S$ as

$$\begin{aligned} \boldsymbol{m}_{ij} &= \phi_m\left(\boldsymbol{h}_i^{(l)}, \boldsymbol{h}_j^{(l)}, f_x(\boldsymbol{X}_i^{(l)}, \boldsymbol{X}_j^{(l)}), e_{ij}\right), \\ \boldsymbol{h}_i^{(l+1)} &= \phi_h\left(\boldsymbol{h}_i^{(l)}, \sum\nolimits_{j \in \mathbb{N}(i)} \boldsymbol{m}_{ij}\right), \\ \boldsymbol{X}_i^{(l+1)} &= \boldsymbol{X}_i^{(l)} + \frac{1}{|\mathbb{N}(i)|} \sum\nolimits_{j \in \mathcal{N}(i)} (\boldsymbol{x}_{i,1}^{(l)} - \boldsymbol{x}_{j,1}^{(l)}) \phi_x(\boldsymbol{m}_{ij}), \end{aligned} \tag{6}$$

where the functions $\phi_m, \phi_h, \phi_x$ are MLPs, $\boldsymbol{x}_{i,1}$ ($\boldsymbol{x}_{j,1}$) denotes the first channel of $\boldsymbol{X}_i$ ($\boldsymbol{X}_j$), $\mathbb{N}(i)$ denotes the spatial neighbors of node $i$, $|\cdot|$ counts the size of the input set, and the invariant message $\boldsymbol{m}_{ij}$ from node $j$ to $i$ is employed to update the invariant feature $\boldsymbol{h}_i^{(l+1)}$ via $\phi_h$ and the equivariant matrix $\boldsymbol{X}_i^{(l+1)}$ via the aggregation of the relative position $\boldsymbol{x}_{i,1}^{(l)} - \boldsymbol{x}_{j,1}^{(l)}$ multiplied with $\phi_x$.

As a core operator in the message passing above, the function $f_x(\boldsymbol{X}_i, \boldsymbol{X}_j)$ is defined as follows:

$$f_x(\boldsymbol{X}_i, \boldsymbol{X}_j) = [\|\boldsymbol{x}_{ij}\|_2, \|\boldsymbol{x}_{ci}\|_2, \|\boldsymbol{x}_{cj}\|_2, \angle_{ci,ij}, \angle_{cj,ij}, \angle_{ci,cj}], \tag{7}$$

where the relative positions are given by $\boldsymbol{x}_{ij} = \boldsymbol{x}_{i,1} - \boldsymbol{x}_{j,1}$, $\boldsymbol{x}_{ci} = \boldsymbol{x}_{i,2} - \boldsymbol{x}_{i,1}$ and $\boldsymbol{x}_{cj} = \boldsymbol{x}_{j,2} - \boldsymbol{x}_{j,2}$; the angles $\angle_{ci,ij}, \angle_{cj,ij}$ and $\angle_{ci,cj}$ are defined as the inner-products of the corresponding vectors denoted in the subscripts, *e.g.* , $\angle_{ci,ij} = \frac{\boldsymbol{x}_{ci} \cdot \boldsymbol{x}_{ij}}{\|\boldsymbol{x}_{ci}\|_2 \|\boldsymbol{x}_{ij}\|_2}$. Through the design in Eq. 7, $f_x(\boldsymbol{X}_i, \boldsymbol{X}_j)$ elaborates the critical information (including relative distances and angles) around the four points: $\boldsymbol{x}_{i,1}, \boldsymbol{x}_{i,2}, \boldsymbol{x}_{j,1}, \boldsymbol{x}_{j,2}$, which largely characterizes the geometrical interaction between the two input matrices. Nicely, $f_x(\boldsymbol{X}_i, \boldsymbol{X}_j)$ is invariant, ensuring the equivariance of Surface-EGNN.

**Dense Attention Output Layer.** Conventionally, we can apply the output of the final layer, *i.e.* , $(\boldsymbol{h}_i^{(L)}, \boldsymbol{X}_i^{(L)})$ to estimate the binding site. Nevertheless, such flat output overlooks the discrepancy of size and shape between different proteins. As showed in Figure 5(b), for small or densely-connected proteins, the receptive field of each node will easily cover most nodes after a small number of message-passing layers, and excessive message passing will lead to over-smoothing (Huang et al., 2020) that will incurs performance detriment. For large or sparsely-connected proteins, on the contrary, insufficient message passing can hardly attain the receptive field with a desirable scope, which will also decrease the performance. It thus requires us to develop an adaptive mechanism to balance the message passing scope between different proteins. We propose the *dense attention output layer* (showed in Figure 4) for this goal.

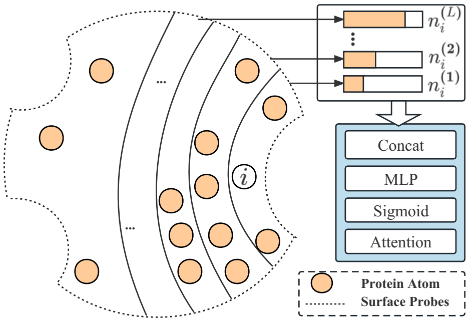

Figure 4: An illustration of Dense Attention.

Intuitively, for each target atom, the spatial distribution of neighbors can reflect the density of spatial connections around. This motivates us to calculate the proportion of atoms with different distance ranges. we take $\theta$ as the distance unit to create the spatial graph and compute by:

$$n_i^{(l)} = \frac{|\{j \in \mathcal{V}_P \mid 0 \leq \|\boldsymbol{x}_i - \boldsymbol{x}_j\|_2 < l\theta\}|}{N_P}, \tag{8}$$

where, the proportion is evaluated within the distance range $[0, l\theta]$, $N_P = |\mathcal{V}_P|$, and the neighbor hop $l \in \mathbb{Z}^+$. We collect the proportions of all hops from 0 to $L$, yielding the proportion vector $\boldsymbol{n}_i = [n_i^{(0)}, n_i^{(1)}, \cdots, n_i^{(L)}, N_P] \in \mathbb{R}^{L+2}$ with $N_P$ plus to emphasize the total number of the protein atoms. Clearly, $\boldsymbol{n}_i$ contains rich information of the spatial density, and we apply it to determine the importance of different layers, by producing the attention $\boldsymbol{a}_i = \text{Sigmoid}(\phi_a(\boldsymbol{n}_i))$. Here, $\phi_a$ is an MLP with the number of output channels as $L+1$, the Sigmoid[1] function is applied for each channel, implying that $\boldsymbol{a}_i \in (0,1)^{L+1}$. Subsequently, we multiply the hidden feature of corresponding layer with each channel of attention vector. The results are then concatenated into a vector denoted as $\boldsymbol{h}_i^{\text{out}}$. To retain translation equivariance, we calculate the mean coordinates of all layers as $\boldsymbol{X}_i^{\text{out}}$:

$$\begin{aligned} \boldsymbol{h}_i^{\text{out}} &= \text{Concat}(a_{i0}\boldsymbol{h}_i^{(0)}, ..., a_{iL}\boldsymbol{h}_i^{(L)}), \\ \boldsymbol{X}_i^{\text{out}} &= \frac{1}{L+1} \sum\nolimits_{l=0}^{L} \boldsymbol{X}_i^{(l)}, \end{aligned} \tag{9}$$

where $a_{il}$ is the $l$-th channel of $\boldsymbol{a}_i$. By making use of Eq. 9, the learnable attentions enable the model to adaptively balance the importance of different layers for different input proteins. We will illustrate the benefit of the proposed strategy in our experiments.

### 3.4. Optimization Objective

**Ligand Binding Site Prediction.** We set $y_i = 1$ if a surface atom $i$ is within 4Å to any ligand atom (Mylonas et al., 2021) and compute $\hat{y}_i = \textbf{Sigmoid}(\text{MLP}(\boldsymbol{h}_i^{\text{out}}))$ as the probability of being a part of binding site according its dense embedding $h_i^{\text{out}}$. The loss $\mathcal{L}_b$ for this task is computed with Dice loss (Jiménez et al., 2017; Kandel et al., 2021).

[1] Note that the sum of $\boldsymbol{a}_i$ is unnecessarily equal to 1, since the Sigmoid function instead of SoftMax function is applied here.

Table 1: Experimental and ablation results of baseline models and our framework.

| Methods | Type | Param | Failure | COACH420 | | HOLO4K | | PDBbind2020 | |
|---|---|---|---|---|---|---|---|---|---|
| | | (M) | Rate ↓ | DCC↑ | DCA↑ | DCC↑ | DCA↑ | DCC↑ | DCA↑ |
| Fpocket[b] | Geometric-based | \ | **0.000** | 0.228 | 0.444 | 0.192 | 0.457 | 0.253 | 0.371 |
| P2rank[b] | Machine-learning | \ | **0.000** | 0.366 | 0.628 | 0.314 | 0.621 | 0.503 | 0.677 |
| DeepSite[b] | CNN-based | 1.00 | \ | \ | 0.564 | \ | 0.456 | \ | \ |
| Kalasanty[b] | | 70.6 | 0.120 | 0.335 | 0.636 | 0.244 | 0.515 | 0.416 | 0.625 |
| DeepSurf[b] | | 33.1 | 0.054 | 0.386 | **0.658** | 0.289 | 0.635 | 0.510 | 0.708 |
| RecurPocket[b] | | 21.2 | 0.075 | 0.354 | 0.593 | 0.277 | 0.616 | 0.492 | 0.663 |
| GAT | Topological Graph | **0.03** | 0.110 | 0.039(0.005) | 0.130(0.009) | 0.036(0.003) | 0.110(0.010) | 0.032(0.001) | 0.088(0.011) |
| GCN | | 0.06 | 0.163 | 0.049(0.001) | 0.139(0.010) | 0.044(0.003) | 0.174(0.003) | 0.018(0.001) | 0.070(0.002) |
| GCN2 | | 0.11 | 0.466 | 0.042(0.098) | 0.131(0.017) | 0.051(0.004) | 0.163(0.008) | 0.023(0.007) | 0.089(0.013) |
| SchNet | Spatial Graph | 0.49 | 0.140 | 0.168(0.019) | 0.444(0.020) | 0.192(0.005) | 0.501(0.004) | 0.263(0.003) | 0.457(0.004) |
| Egnn | | 0.41 | 0.270 | 0.156(0.017) | 0.361(0.020) | 0.127(0.005) | 0.406(0.004) | 0.143(0.007) | 0.302(0.006) |
| EquiPocket-L | Ours | 0.15 | 0.552 | 0.070(0.009) | 0.171(0.008) | 0.044(0.004) | 0.138(0.006) | 0.051(0.003) | 0.132(0.009) |
| EquiPocket-G | | 0.42 | 0.292 | 0.159(0.016) | 0.373(0.021) | 0.129(0.005) | 0.411(0.005) | 0.145(0.007) | 0.311(0.007) |
| EquiPocket-LG | | 0.50 | 0.220 | 0.212(0.016) | 0.443(0.011) | 0.183(0.004) | 0.502(0.008) | 0.274(0.004) | 0.462(0.005) |
| EquiPocket | | 1.70 | 0.051 | **0.423(0.014)** | 0.656(0.007) | **0.337(0.006)** | **0.662(0.007)** | **0.545(0.010)** | **0.721(0.004)** |

[a] The standard deviation of each index is indicated in brackets. The result of 5-fold for EquiPocket is shown in Appendix 12.

[b] We use their published results, codes, or pretrained models. Details in Appendix A.4.6.

**Relative Direction Prediction.** Beyond the CNN-based methods, our EquiPocket is an E(3)-equivariant model, which can not only output the embedding $\boldsymbol{h}_i^{\text{out}}$ but also the coordinate matrix $\boldsymbol{X}_i^{\text{out}}$ (with initial position vector $\boldsymbol{x}_i$). To enhance our framework for gathering local geometric features, we further leverage the position vector $\boldsymbol{m}_i$ to compute the relative direction of its nearest ligand atom by $\boldsymbol{d}_i = \frac{\boldsymbol{m}_i - \boldsymbol{x}_i}{\|\boldsymbol{m}_i - \boldsymbol{x}_i\|_2}$, which is predicted as $\hat{\boldsymbol{d}}_i = \frac{\boldsymbol{x}_i^{\text{out}} - \boldsymbol{x}_i}{\|\boldsymbol{x}_i^{\text{out}} - \boldsymbol{x}_i\|_2}$. The task loss $\mathcal{L}_d$ is computed with cosine loss. We compute the eventual loss by $\mathcal{L} = \mathcal{L}_b + \mathcal{L}_d$.

# 4. Experiments

## 4.1. Settings

**Dataset.** scPDB (Desaphy et al., 2015) is the famous dataset for binding site prediction, which contains the protein, ligand, and 3D cavity structure generated by VolSite (Da Silva et al., 2018). The 2017 release is used for training and cross-validation. PDBbind (Wang et al., 2004) is a commonly used dataset for researching protein-ligand complex, which contains the 3D structures of proteins, ligands, binding sites, and binding affinity results determined in the laboratory. We use the v2020 release for evaluation. COACH 420 and HOLO4K (Kriválk & Hoksza, 2018) are two test datasets for binding site prediction. We use the mlig subsets for evaluation (Mylonas et al., 2021). The data summary and preparation process are detailed in Appendix A.4.

**Target of Binding Sites.** The CNN-based methods (Aggarwal et al., 2021; Jiménez et al., 2017) mark a grid as positive if its distance from the binding site's geometric center is less than 4Å. Following (Mylonas et al., 2021), the protein atoms within 4Å of any ligand atom are set as positive and negative otherwise. After obtaining the probability that an atom is a candidate binding site, we use the mean-shift algorithm (Comaniciu & Meer, 2002) to predict the binding site center, which can determine the number of clusters on its own (details in Appendix A.4.2).

**Evaluation Metrics.**We take the metrics including **DCC** (Distance between the predicted binding site center and the true binding site center), **DCA** (Shortest distance between the predicted binding site center and any grid of the ligand) and **Failures Rate** (Sample rate without any predicted binding site center). Success rate is determined for samples with the DCC(DCA) values below a predetermined threshold. Following (Mylonas et al., 2021), we set the threshold to 4 Å. More details are in Appendix A.4.1.

**EquiPocket Framework.**We implement our framework based on (GAT (Velikovi et al., 2017)+EGNN (Satorras et al., 2021a)) as our global structure modeling module. The probe radius, cutoff $\theta$ and depth of our surface-egnn are set to 1.5, 6 and 4 . To indicate the EquiPocket with different modules, we adopt the following symbol: i) **EquiPocket-L**: Only contain the local geometric modeling module. ii) **EquiPocket-G**: Only contain the global structure modeling module. iii) **EquiPocket-LG**: Only contain both the local geometric and global structure modeling modules. iii) **EquiPocket**: Contain all the modules.

**Baseline Models.**1) geometric-based method: Fpocket (Le Guilloux et al., 2009); 2) machine-learning method: P2rank (Krivák & Hoksza, 2018); 3) CNN-based methods : DeepSite (Jiménez et al., 2017), Kalasanty (Stepniewska-Dziubinska et al., 2020), DeepSurf (Mylonas et al., 2021),

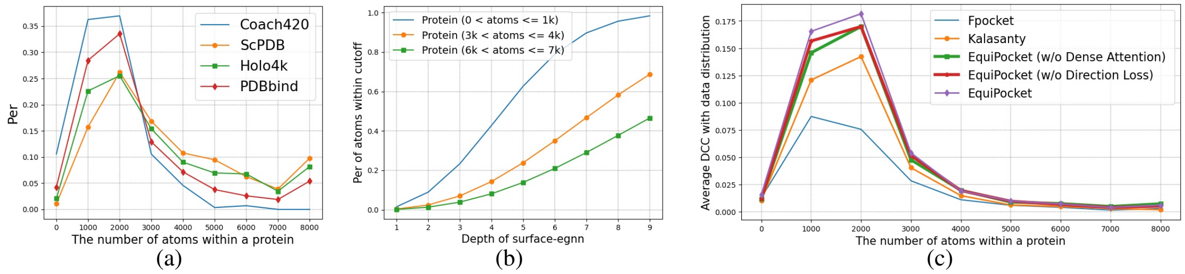

(a) (b) (c)

Figure 5: The protein size shift and model performances for proteins of various sizes

RecurPocket (Li et al., 2022); 4) topological graph-based models: GAT (Velikovi et al., 2017), GCN (Kip & Welling, 2016) and GCN2 (Chen et al., 2020); 5) spatial graph-based models: SchNet (Schütt et al., 2017), EGNN (Satorras et al., 2021b). Detailed implementation in Appendix A.4.6.

### 4.2. Model Comparison

As shown in Table 1, the performance of computational method Fpocket is inferior, with no failure rate, since it simply employs the geometric feature of a protein. The machine-learning method P2rank significantly improves performance by combining Random Forest with geometric info from the protein surface. The performance of CNN-based methods is much superior to that of the computational method, with DCC and DCA improving by more than 50% but requiring enormous parameter and computing resources. However, these two early methods DeepSite and Kalasanty are hampered by protein size shift (Issue 4) and their inability to process big proteins, which may fail prediction. The recently proposed method Deepsurf employs the local-grid concept to handle any size of proteins, although CNN architecture also still results in inevitable failures.

For graph models, the poor performance of topological-graph models (GCN, GAT, GCN2) is primarily because they only consider atom and chemical bond information, ignoring the spatial structure in a protein. The performance of spatial-graph models is generally better than that of topological-graph models. EGNN utilizes not only the properties of atoms but also their relative/absolute spatial positions, resulting in a better effect. SchNet merely updates the embedding of atoms based on the relative distance of atoms. However, the performance of spatial-graph model is worse than that of CNN-based and geometric-based methods because the former cannot obtain enough geometric features (Issue 3) and cannot address the protein size shift (Issue 4).

As the above results indicate, geometric info of protein surface and multi-level structure info in a protein is essential for binding site prediction. In addition, it reflects the limitations of the current GNN models, where it is difficult to collect sufficient geometric information from the protein surface or the calculation resources are too large to apply to macromolecular systems like proteins. Consequently, our EquiPocket framework is not only able to update chemical and spatial information from an atomic perspective but also able to effectively collect geometric information without excessive computing expense, resulting in a 10-20% increase in effect over previous results. Case study for different methods is shown in Appendix A.5.7.

### 4.3. Ablation Study

As shown in Table 1, we conduct ablation experiments on our EquiPocket with different modules.

**Local Geometric Modeling Module.** This module is used to extract the geometric features of protein atoms from their nearest surface probes. EquiPocket-G consists solely of this module, and the performance is negligible. There are two primary causes for this result. First, geometric information can only determine part of the binding sites. Second, it can only reflect the geometric features over a relatively small distance and cannot cover an expansive area.

**Global Structure Modeling Module.** The primary purpose of this module is to extract information about the whole protein, such as atom type, chemical bonds, relevant spatial positions, etc. We implement EquiPocket-G based on (GAT + EGNN) models, which is E(3) equivariance/invariance and has a better effect than its predecessor, EquiPocket-L. In comparison, the value of DCC increased by about 10%, and DCA increased by about 20%. This demonstrates that structure information of the whole protein is necessary for binding site prediction. In addition, when the two modules are combined as the EquiPocket-LG, the performance is significantly improved, proving the complementarity of surface geometric information and global structure information.

**Surface Message Passing Module.** In the previous model, EquiPocket-LG, information was extracted solely from atoms and their closest surface probes. Nonetheless, the binding site is determined not only by the information of a single atom but also by the atoms surrounding it. Therefore, the surface message passing module is proposed to collect

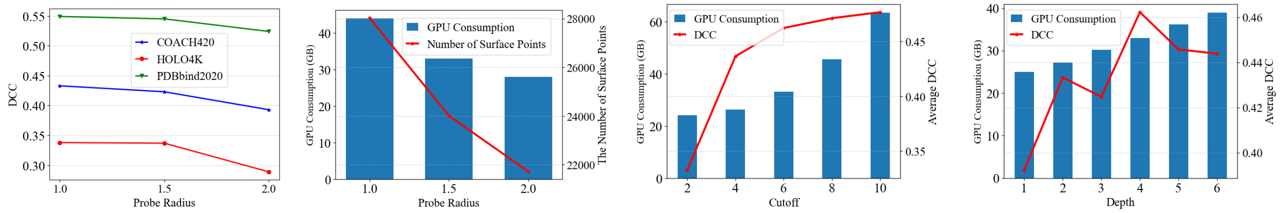

(a) (b) (c) (d)

Figure 6: The influences of the probe radius of MSMS, cutoff $\theta$ and depth of surface-egnn

and update the atom's features from its neighbors. After adding this module, the performance of EquiPocket has been significantly enhanced, DCC and DCA have increased by approximately 20%, and the failure rate has been significantly reduced. Through the addition of multiple modules, we address the Issue 3 and the performance of our framework eventually surpasses that of the existing SOTA method, demonstrating the efficacy of our framework design.

### 4.4. Protein Size Shift

As depicted in the Figure 5(a) and 5(b) that after data processing, there is a significant gap in protein size and distribution between the training dataset (scPDB) and the test dataset (COACH420, HOLO4k, PDBbind). The number of atoms within a protein ranges from hundreds to tens of thousands. As for protein distribution, scPDB has the longest average structure, followed by HOLO4k and PDBbind, with COACH420 having the shortest average protein structure. This fact will hurt model learning and generalization.

We calculate the average DCC with the distribution of various sizes proteins presented in Figure 5(c). The geometric-based method Fpocket performs well for proteins with fewer than 1,000 atoms but degrades as protein size increases. In contrast, the CNN-based method Kalasanty shows performance variations influenced by both protein size and dataset distribution, with a trend of increasing and then decreasing performance. as depicted in Figure 5(a), scPDB shows most proteins contain fewer than 2,000 protein atoms, biasing model parameters. For proteins exceeding 8,000 atoms, Kalasanty underperforms compared to geometric-based methods. The limitation stems from CNN-based methods typically restricting protein space to 70Å * 70Å * 70Å, causing frequent failures with larger proteins. For our EquiPocket framework, we do not need to cut the protein into grids, and we utilize both geometric information from the surface probes and global structure information from the whole protein, so the performance for proteins of varying sizes is significantly superior to that of other methods.

**Dense Attention** is introduced in § 3.3 to reduce the negative impact caused by the protein size shift (Issue 4). As shown in Figure 5(c) (details in Appendix A.5.5), when the number of atoms in a protein is less than 3000, the result of the EquiPocket (w/o Dense Attention) is weaker than that of the original EquiPocket, whereas when the protein is larger, there is no significant distinction between the two models. It simply reflects the role of Dense Attention, which, by weighting the surface-egnn layer at different depths, mitigates the detrimental effect of the protein size shift.

**Direction Loss** is a novel task designed to improve the extraction of local geometric features. The result of the EquiPocket (w/o Direction Loss) in Figure 5(c) demonstrates conclusively that the performance of small proteins with fewer than 3,000 atoms is diminished in the absence of this task, which reveals the importance of the task. The detailed results can be found in Appendix A.5.6.

### 4.5. Hyperparameters Analysis

In our EquiPocket framework, the probe radius of MSMS, the cutoff $\theta$ and depth of surface-egnn are crucial parameters that can impact performance and computational efficiency.

**Probe Radius.** We implement various radius of probe (1, 1.5, 2), which can control the number and density of surface probes. As shown in Figure 6(a) and 6(b), when reducing the radius from 1.5 to 1, the DCC accuracy shows a slight improvement. Conversely, when increasing the radius from 1.5 to 2, the DCC accuracy notably worsens. This is understandable as a smaller radius enhances geometric detail capture on the protein surface, improving pocket detection. Nonetheless, it also increases the number of surface probes, raising GPU memory usage. To strike a balance between memory consumption and detection accuracy, we opt for the default radius value of 1.5 in our experiments. The detailed results are provided in Appendix A.5.1.

**Cutoff $\theta$.** We set the depth of surface-egnn to 4 and implement various cutoff values (2, 4, 6, 8, 10).

Figure 6(c) indicates that with the cutoff set to 2, the average DCC of our framework is poor, and GPU memory is relatively low (22GB). This is due to the fact that when the cutoff is small, the surface-egnn can only observe a tiny receptive field. As the cutoff increases, the performance and GPU memory continue to rise until the DCC reaches a bottleneck when the cutoff is 10, and the GPU memory reaches 62GB. Therefore, when selecting parameters for our framework, we must strike a balance between performance and efficiency.

**Depth.** The depth of surface-egnn has an immediate influences on the performance and computation cost. We set the cutoff to 6 and implement various depth (1, 2, 3, 4, 5, 6). Figure 6(d) demonstrates that as depth increases, performance steadily improves and becomes stable as GPU memory continues to expand. Because the prediction of binding sites is highly influenced by their surrounding atoms, therefore, an excessively large receptive field may not offer any benefits but will necessitate additional computing resources.

## 5. Conclusion

In this paper, concentrating on the ligand binding site prediction, we propose EquiPocket, a novel E(3)-Equivariant geometric graph framework, which contains the local geometric modeling module, global structure modeling module, and surface passing module to gather the surface geometric and multi-level structure features in a protein. Experiments demonstrate that our framework is highly generalizable and beneficial, and achieves superior prediction accuracy and computing efficiency compared with the existing methods.

## Acknowledgements

The work was partially done at Gaoling School of Artificial Intelligence, Beijing Key Laboratory of Big Data Management and Analysis Methods, MOE Key Lab of Data Engineering and Knowledge Engineering, and Pazhou Laboratory (Huangpu), Guangzhou, Guangdong 510555, China. This research was supported in part by the National Science and Technology Major Project under Grant 2020AAA0107300, the National Natural Science Foundation of China (No. U2241212, No. 61932001, No. 62376276), Beijing Natural Science Foundation (No. 4222028), Beijing Outstanding Young Scientist Program (No.BJJWZYJH012019100020098), Beijing Nova Program (20230484278), Alibaba Group through Alibaba Innovative Research Program, and Huawei-Renmin University joint program on Information Retrieval. We also wish to acknowledge the support provided by the fund for building world-class universities (disciplines) of Renmin University of China, by the funds from Engineering Research Center of Next-Generation Intelligent Search and Recommendation, Ministry of Education, from Intelligent Social Governance Interdisciplinary Platform, Major Innovation & Planning Interdisciplinary Platform for the "Double-First Class" Initiative, Renmin University of China, from Public Policy and Decision-making Research Lab of Renmin University of China, and from Public Computing Cloud, Renmin University of China.

## Impact Statement

Our contributions are able to advance the field of machine learning (Ren et al., 2023; Zhou et al., 2024; Jiang et al., 2023; Wang et al., 2023; Xie et al., 2022; Ng et al., 2024), as well as the applications in AI for Science. We do not recognize any significant negative societal impact of this work that should be highlighted here.

## References

Abdollahi, N., Tonekaboni, S. A. M., Huang, J., Wang, B., and MacKinnon, S. Nodecoder: a graph-based machine learning platform to predict active sites of modeled protein structures. *arXiv preprint arXiv:2302.03590*, 2023.

Aggarwal, R., Gupta, A., Chelur, V., Jawahar, C., and Priyakumar, U. D. Deeppocket: ligand binding site detection and segmentation using 3d convolutional neural networks. *Journal of Chemical Information and Modeling*, 2021.

Belgiu, M. and Drăguţ, L. Random forest in remote sensing: A review of applications and future directions. *ISPRS journal of photogrammetry and remote sensing*, 114:24–31, 2016.

Brylinski, M. and Skolnick, J. A threading-based method (findsite) for ligand-binding site prediction and functional annotation. *Proceedings of the National Academy of sciences*, 105(1):129–134, 2008.

Chen, K., Mizianty, M. J., Gao, J., and Kurgan, L. A critical comparative assessment of predictions of protein-binding sites for biologically relevant organic compounds. *Structure*, 19(5):613–621, 2011.

Chen, M., Wei, Z., Huang, Z., Ding, B., and Li, Y. Simple and deep graph convolutional networks, 2020.

Comaniciu, D. and Meer, P. Mean shift: A robust approach toward feature space analysis. *IEEE Transactions on pattern analysis and machine intelligence*, 24(5):603–619, 2002.

Da Silva, F., Desaphy, J., and Rognan, D. Ichem: a versatile toolkit for detecting, comparing, and predicting protein–ligand interactions. *ChemMedChem*, 13(6):507–510, 2018.

Desaphy, J., Bret, G., Rognan, D., and Kellenberger, E. sc-pdb: a 3d-database of ligandable binding sites—10 years on. *Nucleic acids research*, 43(D1):D399–D404, 2015.

Dias, S. E., Nguyen, Q. T., Jorge, J. A., and Gomes, A. J. Multi-gpu-based detection of protein cavities using critical points. *Future Generation Computer Systems*, 67: 430–440, 2017.

Evteev, S. A., Ereshchenko, A. V., and Ivanenkov, Y. A. Siteradar: Utilizing graph machine learning for precise mapping of protein–ligand-binding sites. *Journal of Chemical Information and Modeling*, 63(4):1124–1132, 2023.

Faller, C. E., Raman, E. P., MacKerell, A. D., and Guvench, O. Site identification by ligand competitive saturation (silcs) simulations for fragment-based drug design. In *Fragment-Based Methods in Drug Discovery*, pp. 75–87. Springer, 2015.

Fout, A., Byrd, J., Shariat, B., and Ben-Hur, A. Protein interface prediction using graph convolutional networks. *Advances in neural information processing systems*, 30, 2017.

Gonczarek, A., Tomczak, J. M., Zareba, S., Kaczmar, J., Dabrowski, P., and Walczak, M. J. Learning deep architectures for interaction prediction in structure-based virtual screening. 2016.

Han, J., Rong, Y., Xu, T., and Huang, W. Geometrically equivariant graph neural networks: A survey. 2022.

Hendlich, M., Rippmann, F., and Barnickel, G. Ligsite: automatic and efficient detection of potential small molecule-binding sites in proteins. *Journal of Molecular Graphics and Modelling*, 15(6):359–363, 1997.

Huang, W., Rong, Y., Xu, T., Sun, F., and Huang, J. Tackling over-smoothing for general graph convolutional networks. 2020.

Huang, W., Han, J., Rong, Y., Xu, T., Sun, F., and Huang, J. Equivariant graph mechanics networks with constraints. *arXiv e-prints*, 2022.

Isert, C., Atz, K., and Schneider, G. Structure-based drug design with geometric deep learning. *Current Opinion in Structural Biology*, 79:102548, 2023.

Jiang, M., Wei, Z., Zhang, S., Wang, S., Wang, X., and Li, Z. Frsite: protein drug binding site prediction based on faster r–cnn. *Journal of Molecular Graphics and Modelling*, 93:107454, 2019.

Jiang, N.-F., Zhao, X., Zhao, C.-Y., An, Y.-Q., Tang, M., and Wang, J.-Q. Pruning-aware sparse regularization for network pruning. *Machine Intelligence Research*, 20(1): 109–120, 2023.

Jiménez, J., Doerr, S., Martínez-Rosell, G., Rose, A. S., and De Fabritiis, G. Deepsite: protein-binding site predictor using 3d-convolutional neural networks. *Bioinformatics*, 33(19):3036–3042, 2017.

Kandel, J., Tayara, H., and Chong, K. T. Puresnet: prediction of protein-ligand binding sites using deep residual neural network. *Journal of cheminformatics*, 13(1):1–14, 2021.

Kip, T. N. and Welling, M. Semi-supervised classification with graph convolutional networks. 2016.

Kipf, T. N. and Welling, M. Semi-supervised classification with graph convolutional networks. *arXiv preprint arXiv:1609.02907*, 2016.

Klicpera, J., Giri, S., Margraf, J. T., and Günnemann, S. Fast and uncertainty-aware directional message passing for non-equilibrium molecules. 2020a.

Klicpera, J., Gro, J., and Günnemann, S. Directional message passing for molecular graphs. 2020b.

Kong, X., Huang, W., and Liu, Y. End-to-end full-atom antibody design. *arXiv preprint arXiv:2302.00203*, 2023.

Krivák, R. and Hoksza, D. Improving protein-ligand binding site prediction accuracy by classification of inner pocket points using local features. *Journal of cheminformatics*, 7(1):1–13, 2015.

Krivák, R. and Hoksza, D. P2rank: machine learning based tool for rapid and accurate prediction of ligand binding sites from protein structure. *Journal of cheminformatics*, 10(1):1–12, 2018.

Laskowski, R. A. Surfnet: a program for visualizing molecular surfaces, cavities, and intermolecular interactions. *Journal of molecular graphics*, 13(5):323–330, 1995.

Laurie, A. T. and Jackson, R. M. Q-sitefinder: an energy-based method for the prediction of protein–ligand binding sites. *Bioinformatics*, 21(9):1908–1916, 2005.

Le Guilloux, V., Schmidtke, P., and Tuffery, P. Fpocket: an open source platform for ligand pocket detection. *BMC bioinformatics*, 10(1):1–11, 2009.

Lee, B. and Richards, F. M. The interpretation of protein structures: estimation of static accessibility. *Journal of molecular biology*, 55(3):379–IN4, 1971.

Levitt, D. G. and Banaszak, L. J. Pocket: a computer graphies method for identifying and displaying protein cavities and their surrounding amino acids. *Journal of molecular graphics*, 10(4):229–234, 1992.

Li, P., Cao, B., Tu, S., and Xu, L. Recurpocket: Recurrent lmser network with gating mechanism for protein binding site detection. In *2022 IEEE International Conference on Bioinformatics and Biomedicine (BIBM)*, pp. 334–339. IEEE, 2022.

Liu, Y., Wang, L., Liu, M., Zhang, X., Oztekin, B., and Ji, S. Spherical message passing for 3d graph networks, 2021.

Macari, G., Toti, D., and Polticelli, F. Computational methods and tools for binding site recognition between proteins and small molecules: from classical geometrical approaches to modern machine learning strategies. *Journal of computer-aided molecular design*, 33(10):887–903, 2019.

Meller, A., Ward, M. D., Borowsky, J. H., Lotthammer, J. M., Kshirsagar, M., Oviedo, F., Ferres, J. L., and Bowman, G. Predicting the locations of cryptic pockets from single protein structures using the pocketminer graph neural network. *Biophysical Journal*, 122(3):445a, 2023.

Mylonas, S. K., Axenopoulos, A., and Daras, P. Deepsurf: a surface-based deep learning approach for the prediction of ligand binding sites on proteins. *Bioinformatics*, 37 (12):1681–1690, 2021.

Ng, M. K., Wu, H., and Yip, A. Stability and generalization of hypergraph collaborative networks. *Machine Intelligence Research*, 21(1):184–196, 2024.

Ngan, C.-H., Hall, D. R., Zerbe, B., Grove, L. E., Kozakov, D., and Vajda, S. Ftsite: high accuracy detection of ligand binding sites on unbound protein structures. *Bioinformatics*, 28(2):286–287, 2012.

Ragoza, M., Hochuli, J., Idrobo, E., Sunseri, J., and Koes, D. R. Protein–ligand scoring with convolutional neural networks. *Journal of chemical information and modeling*, 57(4):942–957, 2017.

Rang, H. The receptor concept: pharmacology's big idea. *British journal of pharmacology*, 147(S1):S9–S16, 2006.

Ren, W.-Q., Qu, Y.-B., Dong, C., Jing, Y.-Q., Sun, H., Wu, Q.-H., and Guo, S. A survey on collaborative dnn inference for edge intelligence. *Machine Intelligence Research*, 20(3):370–395, 2023.

Richmond, T. J. Solvent accessible surface area and excluded volume in proteins: Analytical equations for overlapping spheres and implications for the hydrophobic effect. *Journal of molecular biology*, 178(1):63–89, 1984.

Sabrina, Jaeger, Simone, Fulle, Samo, and Turk. Mol2vec: Unsupervised machine learning approach with chemical intuition. *Journal of Chemical Information & Modeling*, 2018.

Sanner, M. F., Olson, A. J., and Spehner, J. C. Reduced surface: An efficient way to compute molecular surfaces. *Peptide Science*, 38(3):305–320, 1996.

Satorras, V. G., Hoogeboom, E., and Welling, M. E(n) equivariant graph neural networks. 2021a.

Satorras, V. G., Hoogeboom, E., and Welling, M. E (n) equivariant graph neural networks. In *International conference on machine learning*, pp. 9323–9332. PMLR, 2021b.

Schütt, K. T., Kindermans, P. J., Sauceda, H. E., Chmiela, S., Tkatchenko, A., and Müller, K.-R. Schnet: A continuous-filter convolutional neural network for modeling quantum interactions. In *Advances in Neural Information Processing Systems*, 2017.

Semwal, R., Aier, I., Tyagi, P., Raj, U., and Varadwaj, P. K. Deeplbs: A deep convolutional neural network-based ligand-binding site prediction tool. In *2023 6th International Conference on Information Systems and Computer Networks (ISCON)*, pp. 1–4. IEEE, 2023.

Stepniewska-Dziubinska, M. M., Zielenkiewicz, P., and Siedlecki, P. Improving detection of protein-ligand binding sites with 3d segmentation. *Scientific reports*, 10(1): 1–9, 2020.

Sun, M., Zhao, S., Coryandar, G., Olivier, E., Zhou, J., and Wang, F. Graph convolutional networks for computational drug development and discovery. *Briefings in Bioinformatics*, 2019.

Tosco, P., Stiefl, N., and Landrum, G. Bringing the mmff force field to the rdkit: implementation and validation. *Journal of Cheminformatics,6,1(2014-07-12)*, 6(1):37, 2014.

Toti, D., Viet Hung, L., Tortosa, V., Brandi, V., and Polticelli, F. Libra-wa: a web application for ligand binding site detection and protein function recognition. *Bioinformatics*, 34(5):878–880, 2018.

Tubiana, J., Schneidman-Duhovny, D., and Wolfson, H. J. Scannet: an interpretable geometric deep learning model for structure-based protein binding site prediction. *Nature Methods*, 19(6):730–739, 2022.

Velikovi, P., Cucurull, G., Casanova, A., Romero, A., Lió, P., and Bengio, Y. Graph attention networks. 2017.

Wang, L., Xu, H., and Kang, W. Mvcontrast: Unsupervised pretraining for multi-view 3d object recognition. *Machine Intelligence Research*, 20(6):872–883, 2023.

Wang, R., Fang, X., Lu, Y., and Wang, S. The pdbbind database: collection of binding affinities for protein-ligand complexes with known three-dimensional structures. *Journal of Medicinal Chemistry*, 47(12):2977–80, 2004.

Weisel, M., Proschak, E., and Schneider, G. Pocketpicker: analysis of ligand binding-sites with shape descriptors. *Chemistry Central Journal*, 1(1):1–17, 2007.

Xie, J., Liu, S.-Y., and Chen, J.-X. A framework for distributed semi-supervised learning using single-layer feedforward networks. *Machine Intelligence Research*, 19(1): 63–74, 2022.

Xu, K., Hu, W., Leskovec, J., and Jegelka, S. How powerful are graph neural networks? 2018.

Yang, Z., Zhong, W., Lv, Q., Dong, T., and Yu-Chian Chen, C. Geometric interaction graph neural network for predicting protein–ligand binding affinities from 3d structures (gign). *The Journal of Physical Chemistry Letters*, 14(8):2020–2033, 2023.

Zhang, Y., Zhou, G., Wei, Z., and Xu, H. Predicting protein-ligand binding affinity via joint global-local interaction modeling. *arXiv preprint arXiv:2209.13014*, 2022.

Zhou, H., Ren, J., Deng, H., Cheng, X., Zhang, J., and Zhang, Q. Interpretability of neural networks based on game-theoretic interactions. *Machine Intelligence Research*, pp. 1–22, 2024.

# A. Appendix

## A.1. The pseudo-code of our EquiPocket framework

**Algorithm 1** EquiPocket

```
Input: Protein structure $\mathcal{G}_P$
Output: Candidate Binding sites and their ligandability score
Clean Structure by removing solvent, hydrogens atoms
Create the solvent accessible surface of the protein $\mathbb{S}$ use MSMS
for every $s_i$ in $\mathbb{S}$ do
    Get its closed protein atom $p_i$
end for
Get the surface atom $\mathcal{V}_S$ according to the surface points‘s closed protein atom
for every surface atom $i \in \mathcal{V}_S$ do
    Get their surrounding surface points set $\mathbb{S}_i$
    Get the geometric embedding $\boldsymbol{g}_i$
end for
Get the global structure embedding $\boldsymbol{c}_i^{''}$ of the protein
for every surface atom $i \in \mathcal{V}_S$ do
    Get its invariant feature $\boldsymbol{h}_i^{(0)} = [\boldsymbol{c}_i'', \boldsymbol{g}_i].]$ and equivariant position matrix $\boldsymbol{X}_i^{(0)} = [\boldsymbol{x}_i, \bar{\boldsymbol{x}}_i]$
    Get the updated embedding $\boldsymbol{h}_i^{(l)}$ and updated coordinates $\boldsymbol{X}_i^{(l)}$ based on our surface-egnn model
    Get the dense embedding $\boldsymbol{h}_i$ and position $\boldsymbol{X}_i$ according to its dense attention $\boldsymbol{a}_i$
    predict the probability $\hat{\boldsymbol{y}}_i$ as ligandability score and the nearest ligand atom direction $\boldsymbol{d}_i$
end for
Discard protein atoms with probability less than T (T=0.5 in our experiments);
Cluster the remaining protein atoms;
Form binding sites and get the average ligandability score for each cluster;
Rank the predicted binding sites by their ligandability score;
return The candidate binding sites and ligandability score;
```

## A.2. Related Work

### A.2.1. Binding Site Prediction

**Computational Methods.** The computational methods for binding site prediction include geometry-based (Levitt & Banaszak, 1992; Hendlich et al., 1997; Weisel et al., 2007; Le Guilloux et al., 2009; Chen et al., 2011; Dias et al., 2017), probe- and energy-based (Laskowski, 1995; Laurie & Jackson, 2005; Ngan et al., 2012) and template-based (Brylinski & Skolnick, 2008; Toti et al., 2018) methods: 1) Since most ligand binding sites occur on the 3D structure, geometry-based methods (POCKET (Levitt & Banaszak, 1992), CriticalFinder (Dias et al., 2017), LigSite (Hendlich et al., 1997), Fpocket (Le Guilloux et al., 2009), etc. ) are designed to identify these hollow spaces and then rank them using the expert design geometric features. 2) Probe-based methods (SURFNET (Laskowski, 1995), Q-SiteFinder (Laurie & Jackson, 2005), etc. (Faller et al., 2015)), also known as energy-based methods, calculate the energy resulting from the interaction between protein atoms and a small-molecule probe, whose value dictates the existence of binding sites. 3)Template-based methods (FINDSITE (Brylinski & Skolnick, 2008), LIBRA (Toti et al., 2018), etc.) are mainly to compare the required query protein with the published protein structure database to identify the binding sites.

**Traditional Learning-based Methods.** PRANK (Krivák & Hoksza, 2015) is a learning-based method that employs the traditional machine learning algorithm random forest(RF) (Belgiu & Drăguţ, 2016). Based on the pocket points and chemical properties from Fpocket (Le Guilloux et al., 2009) and Concavity (Chen et al., 2011), this method measures the "ligandibility" as the binding ability of a candidate pocket using the RF model. P2rank (Krivák & Hoksza, 2018) is a widely used package for locating the ligand-binding pockets based on protein structures, which enhances prediction performance by incorporating geometric information from the protein surface and Random Forest. However, those methods require the manual extraction of numerous features with limit upgrading.

**CNN-based Methods.** Over the last few years, deep learning has surpassed far more traditional ML methods in many domains. For ligand binding site prediction task, many researchers (Jiménez et al., 2017; Stepniewska-Dziubinska et al., 2020; Mylonas et al., 2021; Kandel et al., 2021; Aggarwal et al., 2021) regard a protein as a 3D image, and model this task as a computer vision problem. DeepSite (Jiménez et al., 2017) is the first attempt to employ the CNN architecture for binding site prediction, which like P2Rank (Krivák & Hoksza, 2018) treats this task as a binary classification problem and converts a protein to 3D voxelized grids. The methods FRSite (Jiang et al., 2019) and Kalasanty (Stepniewska-Dziubinska et al., 2020) adhere to the principle of deepsite, but the former regards this task as an object detection problem, and the latter regards this task as a semantic segmentation task. Deeppocket (Aggarwal et al., 2021) is a method similar to p2rank, but implements a CNN-based segmentation model as the scoring function in order to more precisely locate the the binding sites. DeepSurf (Mylonas et al., 2021) constructs a local 3D grid and updates the 3D-CNN architecture to mitigate the detrimental effects of protein rotation. RecurRocket (Li et al., 2022) incorporates recurrent Lmser(Least mean square error reconstruction) networks with CNNs to enhance the representation learning on the 3D protein structures. The recent CNN-based method DeepLBS (Semwal et al., 2023) uses geometrical as well as pharmacophoric properties to quantify the ligand-binding site.

#### A.2.2. Graph Neural Networks for Molecule Modeling

There are multi-level information in molecules including atom info, chemical bonds, spatial structure, physical constraints, etc. Numerous researchers view molecules as topological structures and apply topological-based GNN models (like graph2vec (Gonczarek et al., 2016), GAT (Velikovi et al., 2017), GCN (Kip & Welling, 2016), GCN2 (Chen et al., 2020), GIN (Xu et al., 2018) and etc. (Sun et al., 2019)) to extract the chemical info, which achieve positive outcomes. With the accumulation of structure data for molecules, spatial-based graph models (DimeNet (Klicpera et al., 2020b) , DimeNet++ (Klicpera et al., 2020a), SphereNet (Liu et al., 2021), SchNet (Schütt et al., 2017), Egnn (Satorras et al., 2021a), (Huang et al., 2022), (Han et al., 2022) and etc.) are proposed for molecule task which aggregates spatial and topological information. However, these models may not be adequate for macro-molecules due to their high calculation and resource requirements.

#### A.2.3. GNN-based methods for Pocket Tasks.

ScanNet (Tubiana et al., 2022): This model constructs atom and amino acid representations based on the spatial and chemical arrangement of neighboring entities. It is trained to detect protein-protein and protein-antibody binding sites, showcasing its accuracy even with unseen protein folds. However, it should be noted that ScanNet doesn't incorporate surface geometric information of proteins, and it isn't tailored specifically for ligand-protein datasets. It utilizes a straightforward message passing approach and lacks consideration of geometric invariance. Besides, ScanNet is designed for predicting binding sites in protein and protein, protein and antibody, and protein and disordered protein interactions, making it unsuitable for ligand binding site prediction. PocketMiner (Meller et al., 2023): This model utilizes a geometric graph model to identify cryptic pockets. Unlike our study, PocketMiner doesn't focus on pinpointing where a structure becomes a pocket, which is related to target detection or semantic tasks. Instead, its main goal is predicting the locations where cryptic pockets, already known in advance, will open—a classification prediction task. The evaluation metric used is ROC-AUC, and it is compared against molecular simulation methods. NodeCoder (Abdollahi et al., 2023): NodeCoder is a computational model designed for the prediction of protein residue types based on a geometric graph representation. The model encompasses six distinct residue classifications, namely ligands, peptides, ions, nucleic acid binding sites, post-translational modifications, and transmembrane regions. It is crucial to emphasize that NodeCoder primarily serves as a residue classification tool rather than a protein pocket detection algorithm. SiteRadar (Evteev et al., 2023): This model incorporates the generation of grids, grid clustering, and the application of GNNs to learn geometric information of protein for the mapping of binding sites. PIPGCN (Fout et al., 2017): This model employs GNN model to aggregate information from different protein residues and predict their categories in the Docking Benchmark Dataset. These categories include residues that interact with ligands and those that do not. It's crucial to emphasize that PIPGCN is designed for a classification task rather than target detection or semantic segmentation.

Table 2: Summary of Dataset

| DataSet | Average | | | |
|---|---|---|---|---|
| | Atom Num | Atom in Surface | Surface Points | Target Atoms |
| scPDB | 4205 | 2317 | 24010 | 47 |
| COACH420 | 2123 | 1217 | 12325 | 58 |
| HOLO4k | 3845 | 2052 | 20023 | 106 |
| PDBbind | 3104 | 1677 | 17357 | 37 |

### A.3. Experiment Details

#### A.3.1. Dataset

scPDB (Desaphy et al., 2015) is the famous dataset for binding site prediction, which contains the protein structure, ligand structure, and 3D cavity structure generated by VolSite (Da Silva et al., 2018). The 2017 release of scPDB is used for training and cross-validation of our framework, which contains 17,594 structures, 16,034 entries, 4,782 proteins, and 6,326 ligands. PDBbind (Wang et al., 2004) is a well-known and commonly used dataset for the research of protein-ligand complex. It contains the 3D structures of proteins, ligands, binding sites, and accurate binding affinity results determined in the laboratory. We use the release of v2020, which consists of two parts: general set (14, 127 complexes) and refined set (5,316 complexes). The general set contains all protein-ligand complexes. The refined set contains better-quality compounds selected from the general set, which is used for the test in our experiments. COACH 420 and HOLO4K are two test datasets for the binding site prediction, which are first introduced by (Krivák & Hoksza, 2018). Consistent with (Krivák & Hoksza, 2018; Mylonas et al., 2021; Aggarwal et al., 2021), we use the mlig subsets of each dataset for evaluation, which contain the relevant ligands for binding site prediction.

## A.4. Supplementary Experiment Preparation

We perform the following four processing steps: i) Cluster the structures in scPDB by their Uniprot IDs, and select the longest sequenced protein structures from every cluster as the train data (Kandel et al., 2021). Finally, 5,372 structures are selected out. ii) Split proteins and ligands for the structures in COACH420 and HOLO4k, according to the research (Krivák & Hoksza, 2018) . iii) Clean protein by removing the solvent, hydrogens atoms. Using MSMS (Sanner et al., 1996) to generate the solvent-accessible surface of a protein. iv) Read the protein file by RDKIT (Tosco et al., 2014), and extract the atom and chemical bond features. Remove the error structures.

### A.4.1. Evaluation Metrics

**DCC** is the distance between the predicted binding site center and the true binding site center. **DCA** is the shortest distance between the predicted binding site center and any atom of the ligand. The samples with DCC(DCA) less than the threshold are considered successful. The samples without any binding site center are considered failures. Consistent with (Jiménez et al., 2017; Mylonas et al., 2021; Aggarwal et al., 2021; Stepniewska-Dziubinska et al., 2020), threshold is set to 4 Å. We use **Success Rate** and **Failure Rate** to evaluate experimental performance.

$$\begin{aligned}
&\text{Success Rate(DCC/DCA)} = \\
&\frac{1(\{\text{Predicted sites}|\text{DCC/DCA} < \text{threshold}\})}{1(\{\text{True sites}\})}, \\
&\text{Failure Rate} = \\
&\frac{1(\{\text{Protein}|1(\text{predicted binding center}) = 0\})}{1(\{\text{Protein}\})},
\end{aligned} \tag{10}$$

where $1(\cdot)$ represents the cardinality of a set. After ranking the predicted binding sites, we take the same number with the true binding sites to calculate the success rate.

### A.4.2. Binding sites center

Table 3: The summary of binding sites for the experiment datasets.

| Number of Binding Sites | Number of Proteins | | |
|---|---|---|---|
| | COACH420 | Holo4k | PDBbind |
| 1 | 235 | 2442 | 5025 |
| 2 | 36 | 635 | 0 |
| 3 | 7 | 67 | 0 |
| 4 | 4 | 22 | 0 |
| >=5 | 2 | 38 | 0 |

The CNN-based methods (Jiménez et al., 2017; Aggarwal et al., 2021; Stepniewska-Dziubinska et al., 2020) consider a protein as a 3D image, convert it to a voxel representation by discretizing it into grids and calculate the geometric center of binding site $center_{cnn}$ according to the grid of the cavity or ligand. They label the **grid** as positive if its geometric center is closer than 4Å to the binding sites geometric center. Therefore, the prediction objects of these models actually contain the grid of **ligand atoms**. The predicted binding site center $\hat{center}_{cnn}$ of CNN-based methods is calculated according to the positive grid. For our EquiPocket, we label the **protein atoms** within 4Å of any ligand atom as positive and negative otherwise. Therefore, there is a natural gap in the prediction object between our framework and CNN-based methods, which also lead to the natural gap for the center of predicted binding site. In order to reduce the metric difference caused by the different prediction objects, we get the predicted binding site center $\hat{center}_{equipocket}$ as follow: Ww use $pos_i \in \mathbb{R}^3$ to represent the position of protein atom $v_i$, $center_i \in \mathbb{R}^3$ to represent the nearest surface point center, $\hat{pos}_i^L \in \mathbb{R}^3$ to represent the predicted position of nearest ligand atom from the protein atom $v_i$. The $p\hat{o}s_i^L$ is used to calculate the geometric center of binding site.

$$\widehat{pos}_i^L = pos_i + threshold \cdot \frac{(center_i - pos_i)}{|center_i - pos_i|}, \tag{11}$$

Where $threshold4$ is set to 4, because we label the protein atoms within **4Å** of any ligand atom as positive and negative otherwise.

### A.4.3. Experiment Process

As indicated by the data distribution presented in Table A.4.2, the majority of samples in the test dataset consist of a single binding site, with only a subset of samples containing multiple binding sites.

Following related methods (Krivák & Hoksza, 2018; Jiménez et al., 2017; Mylonas et al., 2021; Aggarwal et al., 2021; Le Guilloux et al., 2009), the specific processing steps of our method are outlined belowr:

**Training Process**:

a. Following DeepSurf (Mylonas et al., 2021), the protein atoms within 4 Ångströms of any ligand atom are set as positive, otherwise negative.

b. EquiPocket predicts the druggability probability for each atom, using the Dice loss function for model optimization.

**Validation and Testing**:

a. In accordance with related methods (Krivák & Hoksza, 2018; Jiménez et al., 2017; Mylonas et al., 2021; Aggarwal et al., 2021; Le Guilloux et al., 2009), we define the center of a binding site as the mean position of the ligand atoms. This definition allows us to handle the proteins with multiple binding sites ($N \geq 1$).

b. We focus on predicting druggability probabilities for each atom rather than identifying specific binding site atoms.

c. Our method uses predicted atom-level probabilities in a clustering process (Comaniciu & Meer, 2002) to autonomously identify ligand binding site centers and druggability, which are crucial for metrics and downstream docking tasks.

**Performance Evaluation**:

a. We evaluate based on the top-$n$ predicted binding site centers, where $n$ does not exceed the actual number of binding sites. If no predicted binding sites center is found, it is considered a failure.

b. The predicted ligand binding center with the DCC/DCA falls below a predetermined threshold, typically set to 4, is classified as successful.

Through the aforementioned process, we are able to effectively handle proteins with more than one binding site during training, validation, and testing.

### A.4.4. Cross-validation

We shuffled the training data and divided the data into 5 parts, taking one of them at a time as the validation set. We use 5-fold cross-validation and report the mean and standard deviation. we present detailed results in Table 12.

### A.4.5. Environment and Parameter Settings

For geometric-based method Fpocket, we use its published tool. For CNN-based methods kalasanty and DeepSurf, we use their published pre-train models. For GNN-based models, the number of layers is set to 3 except GAT. For GAT, we set the number to 1. For GIN, we set the initial $\epsilon$ to 0 and make it trainable. For GCN2, we set the strength of the initial residual connection $\alpha$ to 0.5 and the strength of the identity mapping $\beta$ to 1. For SchNet, EGNN, DimeNet++, SphereNet as baseline models, we set the cutoff distance to 5. For our EquiPocket, we use Adam optimizer for model training with a learning rate of 0.0001 and set the batch size as 8. The basic dimensions of node and edge embeddings are both set to 128. The dropout rate is set to 0.1. The probe radius in MSMS to generate solvent-accessible surface of a protein is set to 1.5. We implement our EquiPocket framework in PyTorch Geometric, all the experiments are conducted on a machine with an NVIDIA A100 GPU (80GB memory). We take 5-fold cross validation on training data scPDB and use valid loss to save checkpoint.

### A.4.6. Baseline Results and Codes

Table 4 describes sources of baseline codes. The results of DeepSite come from (Mylonas et al., 2021). We utilize the published pretrained models of kalasanty (Stepniewska-Dziubinska et al., 2020), DeepSurf (Mylonas et al., 2021) for test results. RecurPocket (Li et al., 2022) has made updates on two existing models: kalasanty and DeepPocket. The former is a pure CNN-based method, while the latter relies on the geometry-based method Fpocket to identify candidate pockets and then utilizes CNNs for ranking. To ensure a fair comparison, we chose to test with the former pretrained model of RecurPocket (kalasanty). The recent CNN-based method DeepLBS (Semwal et al., 2023) did not provide pretrained models or public codes, so it was not included in the baselines. The machine-learning method P2Rank (Krivák & Hoksza, 2018) was originally trained on the CHEN11 and JOINED datasets (Krivák & Hoksza, 2018), totaling 792 samples. In contrast, deep learning methods such as DeepSite, Kalasanty, DeepSurf, and EquiPocket commonly used the scPDB dataset (Desaphy et al., 2015) for training, which had 5000 samples after processing and deduplication. P2Rank's paper highlighted the greater diversity of CHEN11 and JOINED compared to scPDB, affecting model performance. To ensure a fair comparison, we attempted to retrain P2Rank on the scPDB dataset. However, as indicated in Table 5, we encountered convergence issues when the training set size exceeded 3000 samples. Therefore, we report the test results of retrained P2rank based on a randomly selected subset of 792 samples from the scPDB, which matches the quantity of number to the CHEN11 and JOINED datasets of P2rank papers.

Table 4: Sources of baseline codes and pre-train models.

| Methods | URL |
|---|---|
| Fpocker | https://github.com/Discngine/fpocket |
| kalasanty | https://gitlab.com/cheminfIBB/kalasanty |
| DeepSurf | https://github.com/stemylonas/DeepSurf |
| RecurPocket | https://github.com/CMACH508/RecurPocket |
| P2rank | https://github.com/rdk/p2rank |
| GAT | https://github.com/pyg-team/pytorch_geometric |
| GCN | https://github.com/pyg-team/pytorch_geometric |
| GCN2 | https://github.com/chennnM/GCNII |
| SchNet | https://github.com/pyg-team/pytorch_geometric |
| EGNN | https://github.com/vgsatorras/egnn/ |

Table 5: The detailed DCA results of retrained P2rank.

| Samples of scPDB | COACH420 | HOLO4k | PDBbind2020 |
|---|---|---|---|
| 100 | 0.611 | 0.602 | 0.655 |
| 1000 | 0.648 | 0.613 | 0.672 |
| 2000 | 0.639 | 0.622 | 0.671 |
| 3000 | 0.177 | 0.130 | 0.256 |
| 4000 | 0.177 | 0.130 | 0.256 |
| 5000 | 0.177 | 0.130 | 0.256 |

Table 6: Experimental results with different probe radius by MSMS.

| Radius | Surface Points | GPU | Failure Rate | COACH420 | HOLO4K | PDBbind2020 |
|---|---|---|---|---|---|---|
| 1 | 28030 | 44 | 0.053 | 0.433(0.018) | 0.338(0.008) | 0.549(0.005) |
| 1.5 | 24010 | 33 | 0.051 | 0.423(0.014) | 0.337(0.006) | 0.545(0.010) |
| 2 | 21725 | 28 | 0.096 | 0.393(0.024) | 0.289(0.004) | 0.524(0.012) |

## A.5. Supplementary Experimental Results

### A.5.1. Probe Radius

To evaluate the sensitivities of this parameter, we implement various radius of probe (1, 1.5, 2) and provide the number of surface points, GPU memory consumption, failure rate, and the DCC accuracy of our EquiPocket on the test sets in Table 6.

### A.5.2. The inference speed of different methods

Table 7: The inference speed of different methods.

| Method | Type | Time (s) per 100 proteins | Average DCC |
|---|---|---|---|
| fpocket | Geometric-based | 23 | 0.214 |
| Kalasanty | 3D-CNN | 86 | 0.321 |
| DeepSurf |  | 641 | 0.366 |
| EquiPocket | Ours | 37 | 0.431 |

As showed in Table 7, the comparison of various methods for predicting 100 proteins reveals the following: fpocket: Fastest with only 23 seconds for 100 proteins, leveraging manually defined geometric features. However, its performance metrics are not notable. Kalasanty and DeepSurf: Both are 3D-CNN-based. DeepSurf, using detailed local grids on protein surfaces, outperforms Kalasanty in metrics but is slower and the least efficient among the methods compared. EquiPocket: Our method takes 47 seconds per 100 proteins and shows the best DCC metrics. It's faster than 3D-CNN methods but slower than geometric-based ones. This is due to 3D-CNN methods transforming proteins into 3D images (eg. 36 * 36 * 36 grids), increasing computational costs compared to our using atom information (averages 2000-3000 nodes in a protein). EquiPocket also integrates surface features with Surface-EGNN, enhancing efficiency over DeepSurf.

### A.5.3. The informative ablation experiment for our two feature extractors.

Table 8: The informative ablation experiment for our two feature extractors.

|  |  | COACH420 |  | HOLO4k |  | PDBbind |  |
|---|---|---|---|---|---|---|---|
| Model | Fail Ratio | DCC | DCA | DCC | DCA | DCC | DCA |
| EquiPocket/L | 0.13 | 0.355 | 0.546 | 0.296 | 0.574 | 0.465 | 0.606 |
| EquiPocket/R | 0.09 | 0.364 | 0.541 | 0.294 | 0.598 | 0.474 | 0.627 |
| EquiPocket/LR | 0.16 | 0.308 | 0.502 | 0.268 | 0.543 | 0.409 | 0.566 |
| EquiPocket | 0.05 | 0.423 | 0.656 | 0.337 | 0.662 | 0.545 | 0.721 |

Our model predominantly comprises two feature extractors: local geometric modeling module and global structural modeling module, subsequently followed by the surface-EGNN model. In response to your valuable suggestion, we propose the following definitions:

EquiPocket/L: This variant of EquiPocket excludes local geometric modeling module.

EquiPocket/R: This variant of EquiPocket excludes global structural modeling module.

EquiPocket/LR: This variant of EquiPocket excludes both local geometric modeling module and global structural modeling module.

The results in Table 8 indicate that omitting any of these modules negatively impacts performance. Specifically, excluding either the local geometric (L) or global structural (R) module leads to a 10%-15% decrease in DCC/DCA metrics; removing both L and R modules results in a more significant drop of 20%-25%. These results highlight the essential role of both feature extractors in predicting ligand binding sites. Notably, the more pronounced performance decline when omitting the local geometric module (L) suggests its higher importance in protein pocket prediction. This finding is consistent with current trends where methods like Fpocket, P2rank, and DeepSurf primarily utilize geometric features for binding site prediction.

### A.5.4. The comparison results for local geometric features

In Eq. 3 of main paper, $\boldsymbol{g}_i$ is the geometric embedding for a protein atom, learned from surrounding surface probes, and $s_i$ denotes the local geometric properties of these probes with properties such as distances and angle to protein atoms, the surface center, neighboring probes, and so on. Initially, we apply an MLP to these features, followed by pooling. This process transforms the geometric properties before aggregating them into the protein node's geometric embedding. However, since each property of $s_i$ itself carries meaningful information. We are concerned that applying MLP first and then pooling might weaken the transmission of this information. Therefore, we take the second part of the equation. To highlight the effectiveness of the features in Eq. 3, we carried out extra experiments with "EquiPocket-former" focusing on the equation's initial part and "EquiPocket-latter" on its latter part. The results in Table 9 indicate:

Table 9: The comparison results for local geometric features

|  |  | COACH420 |  | HOLO4k |  | PDBbind |  |
|---|---|---|---|---|---|---|---|
| Model | Fail Ratio | DCC | DCA | DCC | DCA | DCC | DCA |
| EquiPocket-former | 0.16 | 0.389 | 0.606 | 0.330 | 0.637 | 0.507 | 0.660 |
| EquiPocket-latter | 0.16 | 0.407 | 0.617 | 0.319 | 0.644 | 0.529 | 0.676 |
| EquiPocket | 0.05 | 0.423 | 0.656 | 0.337 | 0.662 | 0.545 | 0.721 |

Using either feature alone diminishes the predictive performance compared to the full EquiPocket model. Specifically, ”EquiPocket-former” alone sees about a 10% drop, while ”EquiPocket-latter” alone results in around a 5% reduction. This outcome underscores the necessity of both features, with the latter part having a more substantial impact on our model’s performance.

### A.5.5. The detailed experiment results of dense attention

In Figure 5(c), we compared EquiPocket with/without the Dense Attention module. We removed the Attention Module in EquiPocket (w/o attention) for this comparison. As showed in Table 10 showed, it is evident that Dense Attention notably improves prediction for proteins with less than 4000 nodes. However, for larger proteins, exceeding 4000 nodes, there’s no significant performance difference. These findings highlight that Dense Attention boosts predictive accuracy for smaller proteins while maintaining performance for larger ones.

Table 10: The detailed DCC results of Dense Attention.

| Atom Num | Protein Num | Ratio | Cumsum Ratio | EquiPocket(w/o Attention) | EquiPocket |
|---|---|---|---|---|---|
| 0-1000 | 296 | 0.04 | 0.04 | 0.328 | 0.428 |
| 1000-2000 | 2193 | 0.27 | 0.3 | 0.547 | 0.621 |
| 2000-3000 | 2534 | 0.31 | 0.61 | 0.551 | 0.590 |
| 3000-4000 | 1143 | 0.14 | 0.75 | 0.343 | 0.388 |
| 4000-5000 | 619 | 0.08 | 0.82 | 0.261 | 0.255 |
| >=5000 | 1440 | 0.18 | 1 | 0.161 | 0.153 |

### A.5.6. The detailed experiment results of Direction Loss

The relative direction between a protein atom and its nearest ligand atom effectively captures the local geometric information of the binding sites on a protein. Different from the previous work (Krivák & Hoksza, 2018; Jiménez et al., 2017; Mylonas et al., 2021), our method can output E(3)-equivariant coordinates. To better capture the geometric details of the protein surface, we introduced more detailed relative direction (direction loss) as a supplementary target.

The corresponding ablation results have been shown in Figure 5(c) in the main paper, and detailed results are presented in Table 11. EquiPocket (w/o Direction Loss) represents our EquiPocket method removing the relative direction prediction module. It can be observed that when the relative direction prediction module is removed, our method’s performance drops for proteins of different sizes. This is especially notable for proteins with fewer than 3000 atoms, which account for 60% of the samples. If the relative direction prediction is removed, the performance drops by approximately 10%. These results demonstrate the effectiveness of our designed relative direction target.

Table 11: The detailed DCC results of Direction Loss.

| Atom_num | Protein num | Ratio | Cumsum ratio | EquiPocket(w/o Direction Loss) | EquiPocket |
|---|---|---|---|---|---|
| 0-1000 | 296 | 0.04 | 0.04 | 0.319 | 0.428 |
| 1000-2000 | 2193 | 0.27 | 0.3 | 0.587 | 0.621 |
| 2000-3000 | 2534 | 0.31 | 0.61 | 0.551 | 0.590 |
| 3000-4000 | 1143 | 0.14 | 0.75 | 0.371 | 0.388 |
| 4000-5000 | 619 | 0.08 | 0.82 | 0.258 | 0.255 |
| >=5000 | 1440 | 0.18 | 1 | 0.144 | 0.153 |

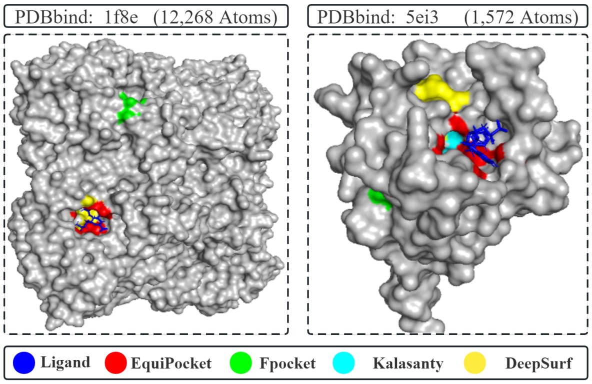

Figure 7: Case Study.

### A.5.7. Case Study

We also display two examples of our EquiPocket and other methods in Figure 7. We take two proteins, 1f8e (with 12,268 atoms) and 5ei3 (with 1,572 atoms), from the test dataset PDBbind. As can be seen from Figure 7: The binding sites predicted by the geometry-based method Fpocket are extremely distant from the actual binding sites. This is due to the fact that this method prioritizes local geometric information and disregards the multi-level structure information of proteins, resulting in limited scope and weak performance. The CNN-based method Kalasanty did not provide any predicted binding site for protein 1f8e. We conjecture that this method restricts the protein within a specific space size which is highly susceptible to failure with large proteins. The recently-proposed CNN-based method DeepSurf takes local grids on the protein surface, which can address the issue of fixed space size. However, the prediction of binding sites in protein 5ei3 by DeepSurf is far from the ground truth because the CNN-based methods are defective in obtaining geometric and chemical features. Our EquiPocket framework is unaffected by the shortcomings of the aforementioned methods, allowing it to achieve superior outcomes for both large and small proteins.

Table 12: The 5-fold results for EquiPocket.

| Methods | Fold | Param | failure | COACH420 | | HOLO4K | | PDBbind2020 | |
|---|---|---|---|---|---|---|---|---|---|
| | | (M) | Rate ↓ | DCC↑ | DCA↑ | DCC↑ | DCA↑ | DCC↑ | DCA↑ |
| EquiPocket-L | 0 | 0.15 | 0.598 | 0.083 | 0.160 | 0.038 | 0.128 | 0.049 | 0.124 |
| EquiPocket-L | 1 | 0.15 | 0.557 | 0.064 | 0.165 | 0.046 | 0.138 | 0.055 | 0.142 |
| EquiPocket-L | 2 | 0.15 | 0.571 | 0.074 | 0.177 | 0.045 | 0.139 | 0.052 | 0.122 |
| EquiPocket-L | 3 | 0.15 | 0.462 | 0.059 | 0.173 | 0.042 | 0.138 | 0.052 | 0.129 |
| EquiPocket-L | 4 | 0.15 | 0.472 | 0.072 | 0.180 | 0.048 | 0.146 | 0.049 | 0.143 |
| EquiPocket-G | 0 | 0.42 | 0.305 | 0.135 | 0.330 | 0.122 | 0.400 | 0.142 | 0.302 |
| EquiPocket-G | 1 | 0.42 | 0.291 | 0.175 | 0.385 | 0.128 | 0.405 | 0.145 | 0.302 |
| EquiPocket-G | 2 | 0.42 | 0.295 | 0.145 | 0.357 | 0.121 | 0.407 | 0.145 | 0.305 |
| EquiPocket-G | 3 | 0.42 | 0.278 | 0.169 | 0.367 | 0.127 | 0.406 | 0.133 | 0.292 |
| EquiPocket-G | 4 | 0.42 | 0.292 | 0.152 | 0.367 | 0.133 | 0.411 | 0.151 | 0.308 |
| EquiPocket-LG | 0 | 0.50 | 0.235 | 0.225 | 0.442 | 0.183 | 0.498 | 0.273 | 0.463 |
| EquiPocket-LG | 1 | 0.50 | 0.207 | 0.220 | 0.460 | 0.189 | 0.509 | 0.280 | 0.468 |
| EquiPocket-LG | 2 | 0.50 | 0.203 | 0.184 | 0.440 | 0.180 | 0.510 | 0.269 | 0.459 |
| EquiPocket-LG | 3 | 0.50 | 0.224 | 0.215 | 0.448 | 0.186 | 0.500 | 0.275 | 0.465 |
| EquiPocket-LG | 4 | 0.50 | 0.231 | 0.213 | 0.431 | 0.179 | 0.492 | 0.272 | 0.456 |
| EquiPocket | 0 | 1.70 | 0.054 | 0.423 | 0.656 | 0.341 | 0.665 | 0.558 | 0.715 |
| EquiPocket | 1 | 1.70 | 0.053 | 0.431 | 0.660 | 0.329 | 0.668 | 0.538 | 0.725 |
| EquiPocket | 2 | 1.70 | 0.041 | 0.443 | 0.664 | 0.336 | 0.660 | 0.550 | 0.724 |
| EquiPocket | 3 | 1.70 | 0.051 | 0.411 | 0.646 | 0.338 | 0.668 | 0.532 | 0.723 |
| EquiPocket | 4 | 1.70 | 0.053 | 0.407 | 0.654 | 0.345 | 0.652 | 0.546 | 0.719 |